Persistent Luminescence Nanosensors: A Generalized Optode-based Platform for Autofluorescence-free Sensing in Biological Systems

Tyler Z. Sodia[1], Hanna L. Tetu[2], Samuel C. Saccomano[3], Elizabeth G. Letch[1], John M. Branning, Jr.[1,4], Adrian A. Mendonsa[3], Shubham Vyas[2], Kevin J. Cash[*1,3]

1) Quantitative Biosciences and Engineering Program. Colorado School of Mines, Golden, CO 80401

2) Department of Chemistry. Colorado School of Mines, Golden, CO 80401

3) Department of Chemical and Biological Engineering. Colorado School of Mines, Golden CO 80401

4) The MITRE Corporation, Bedford, Massachusetts, United States of America. The author's affiliation with The MITRE Corporation is for identification purposes only and is not intended to convey or imply MITRE's concurrence with, or support for, the positions, opinions, or viewpoints expressed by the author. Approved for Public Release, Distribution Unlimited. Public Release Case Number 24-0224.

ABSTRACT: Fluorescent nanosensors have drastically progressed our ability to accelerate diagnostics and quantify cellular dynamics in real time. Their modular assembly allows for facile sensor tuning, leading to a large expansion of analytes and systems that can be analyzed. Still, separating sensor signals from background optical signatures remains a major hurdle in the field. Exploiting this modular synthesis, we merged optode-based sensing with near-infrared emitting $ZnGa_2O_4:Cr^{3+}$ persistent luminescence nanoparticles (PLNPs) to create functional nanocomposites for autofluorescence-free "glow-in-the-dark" sensing. We hydrophobically modified the PLNP surface with covalently bound ligands and incorporated the PLNPs into the polymeric core of optode-based nanoparticles. We demonstrate persistent luminescence nanosensors (PLNs) for five different analytes (K^+, Na^+, Ca^{2+}, pH, and O_2) based on two different sensing mechanisms. The PLNs allowed us to achieve autofluorescence-free quantification of K^+ in fetal bovine serum and ratiometric metabolic monitoring of microbial samples with time-resolved luminescence acquisition. We foresee that this approach will allow for high signal-to-noise ratios while sensing in optically challenging samples.

Nanoparticle-based optical sensors (nanosensors) are useful tools for probing chemical and biological systems(1–3). Because native fluorescent molecules tend to interfere with quantitative analysis, persistent luminescence nanoparticles (PLNPs) are emerging as a popular probe for optical sensing(4–6). Instead of separating sensor signal from background by wavelength, the long-lasting emission of PLNPs (which is orders of magnitude longer than typical luminophores(7–9)) allows for temporal signal separation with a time-resolved acquisition. By attaching recognition elements to the PLNP, autofluorescence-free sensing with PLNPs has been achieved for proteins, nucleic acids, and small biomolecules(10–13).

Another notable class of nanosensors are those derived from the polymeric optode membrane that function on target analyte partitioning and its interactions with the chemical moieties embedded in the particle's hydrophobic core(14). This two-phase architecture allows for facile switching of the loaded components to sense a different analyte or tuning optical properties(14–16). Importantly, this enables the incorporation of luminescent nanomaterials into the sensor matrix(15) e.g. CdSe/ZnS core-shell quantum dots(17), upconversion $NaYF_4$:Er,Yb nanorods(18), silicon nanocrystals(19), and graphene carbon dots(20, 21). In 2019, our group developed a Na^+ selective optode membrane that incorporated a persistent luminescent microparticle(22). Due to the μm size of the particles, this approach precluded nanosensor fabrication which limits both response time and application in many biological systems.

Here, we merged optode-based sensing with persistent luminescence nanoparticles to create functional nanocomposites that we term persistent luminescent nanosensors (PLNs). Using flash nanoprecipitation, we integrated hydrophobically modified chromium-doped zinc gallate ($ZGO:Cr^{3+}$) PLNPs into optode-based, polymer nanoparticles for autofluorescence-free signal acquisition and quantification. We demonstrate two sensing

https://doi.org/10.26434/chemrxiv-2024-m0sk6 **ORCID:** https://orcid.org/0000-0002-3198-3340 Content not peer-reviewed by ChemRxiv. **License:** CC BY 4.0

schemes that integrate the ZGO:Cr^{3+}. The first, a traditional ionophore-based approach(14), couples the ZGO:Cr^{3+} persistent luminescence to the variable absorption of a lipophilic pH indicator. By including a selective ionophore for K^+, Na^+, or Ca^{2+}, the absorption/protonation of the indicator becomes dependent on the activity of the respective ion in the aqueous phase, and we demonstrate four different sensors based on the same architecture (**Scheme 1A**)(14). The second sensing scheme is a design for ratiometric, time-resolved O_2 sensing by using the ZGO:Cr^{3+} persistent luminescence as an internal standard signal to the O_2 sensitive, phosphorescent emission of Palladium-TPTBP (**Scheme 1B**). For both systems, by using a time-resolved approach (**Scheme 1C**), we can exclude autofluorescence from biological samples and measure the sensor signal directly, even with significant spectral overlap.

Scheme 1. Sensing Mechanisms

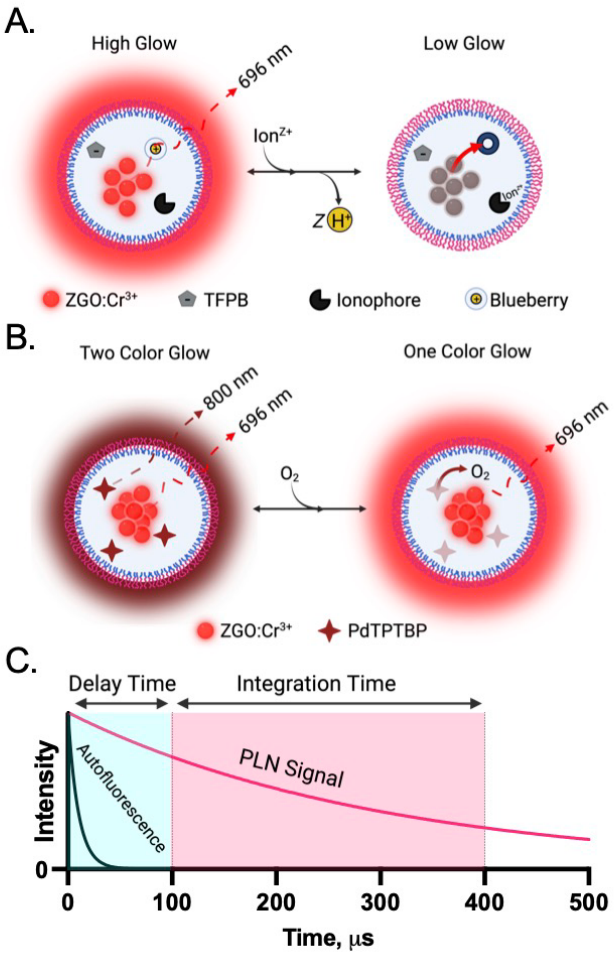

[a] A) Ion-selective PLN mechanism: ions in the surrounding bulk phase displace a proton from the pH-sensitive blueberry dye, increasing its absorbance which gates the persistent luminescence of ZGO:Cr^{3+} B) O_2 PLN mechanism: a ratiometric readout where PdTPTBP is dynamically quenched by O_2 while the ZGO:Cr^{3+} is unaffected by O_2. C) Approach for time-resolved luminescence detection with PLNs.

We synthesized the persistent luminescent ZGO:Cr^{3+} hydrothermally to yield cubic phase nanocrystals with diameters of 10 ± 2nm (**Figure 1A-D**) and a zeta potential of 34 ± 1.1 mV – making the particles easily dispersed in water. The luminescence spectrum in **Figure 1E** at 696nm is the emission of the spin-forbidden $^2E \rightarrow {}^4A_2$ transition of Cr^{3+} (5). As expected, the ZGO:Cr^{3+} NPs have 3 excitation bands (**Figure S1**) – 254 nm, 420 nm, and 580 nm representing the d-d transitions of Cr^{3+} (5). Using a pulse excitation of 420 nm, the Cr^{3+} emission peak showed a multiexponential decay and an effective luminescence lifetime (τ_{eff}) of 531 μs using equation S1. The luminescence decay at 696nm proceeds well into the millisecond range after either a 420 nm (**Figure 1F**) or 266 nm (**Figure S2**) pulse excitation, deeming the ZGO:Cr^{3+} ready for the next steps towards incorporation into our optode-based persistent luminescence sensing approach.

https://doi.org/10.26434/chemrxiv-2024-m0sk6 **ORCID:** https://orcid.org/0000-0002-3198-3340 Content not peer-reviewed by ChemRxiv. **License:** CC BY 4.0

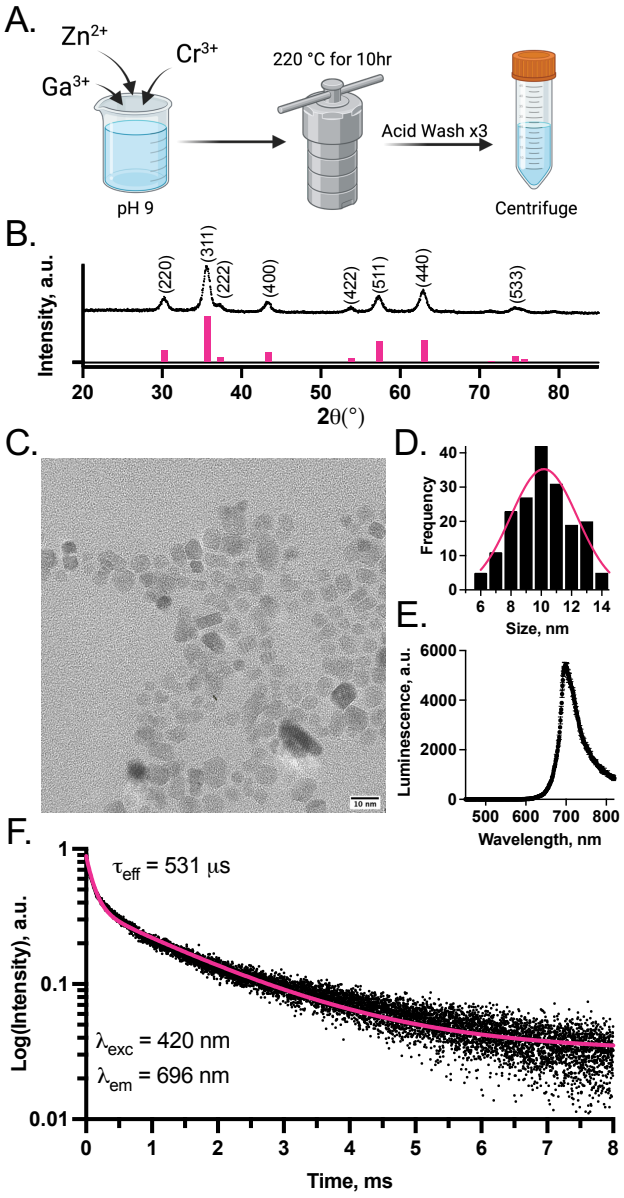

Figure 1. PLNP Characterization. A) Schematic of hydrothermal synthesis and processing. B) X-ray diffraction pattern showing pure cubic spinel structure (ICDD = 00-038-1240). C) HR-TEM image of ZGO:Cr^{3+} (scale bar = 10nm). D) Frequency distribution of ZGO:Cr^{3+} PLNPs (obtained from 200 particles). E) Luminescence spectrum of ZGO:Cr^{3+} after 420nm excitation. F) Luminescence decay of ZGO:Cr^{3+} after 420nm pulse excitation.

In most biological applications, modifications are needed to link recognition sites and/or stabilizing agents to the ZGO:Cr^{3+} surface for sensing or better aqueous stability(4, 5, 23). However, to incorporate our ZGO:Cr^{3+} PLNPs they must have a hydrophobic surface to be retained in the organic phase of the optode-based nanosensor. Thus, the raw ZGO:Cr^{3+} NPs were modified by condensation of trimethoxy(octyl) silane to the hydroxide surface of ZGO:Cr^{3+} NPs (**Figure 2A**) to yield ZGO:Cr^{3+}@TMOS that are stable in nonpolar environments like the optode matrix. The modification was confirmed with Fourier transform infrared (FT-IR) spectroscopy where the peaks in the siloxane region (1090 cm^{-1}, 1053 cm^{-1}, 1033 cm^{-1}, and 1015 cm^{-1}) represent the Si–O–Si stretching, indicating successful condensation and the bands at 2958 cm^{-1}, 2923 cm^{-1}, and 2855 cm^{-1} represent the C(sp^3)-H bonds of the octyl silane attachment protruding from the particle the surface (**Figure 2B**). After ligand addition, the ZGO:Cr^{3+}@TMOS can be dispersed in a variety of organic solvents (THF, chloroform, toluene) for further use.

https://doi.org/10.26434/chemrxiv-2024-m0sk6 **ORCID:** https://orcid.org/0000-0002-3198-3340 Content not peer-reviewed by ChemRxiv. **License:** CC BY 4.0

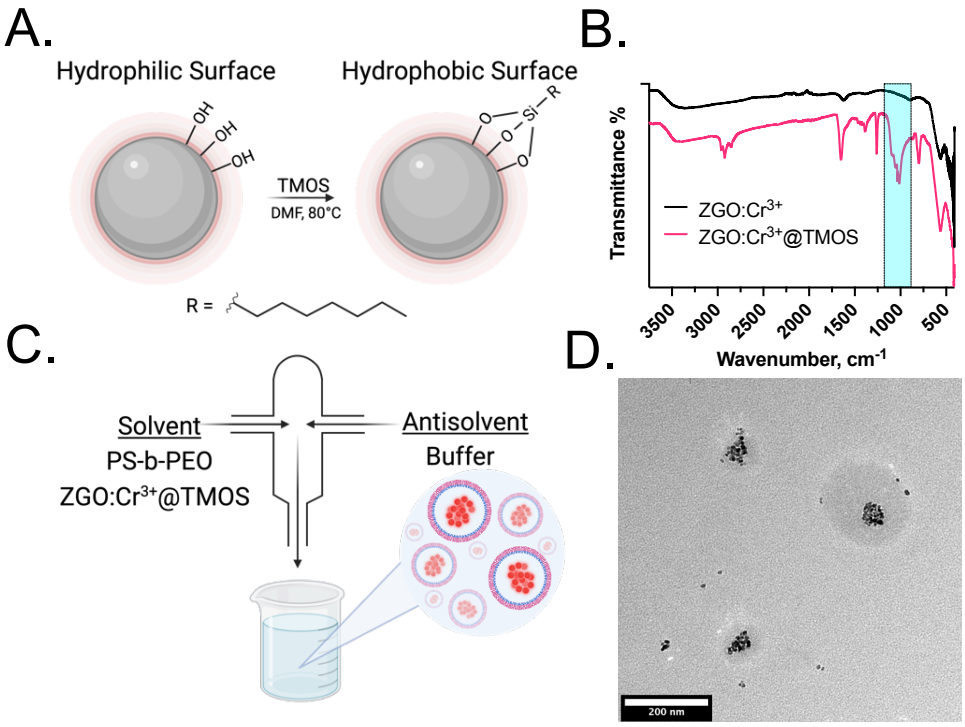

Figure 2. Surface modification of the ZGO:Cr^{3+} NPs and their incorporation into a polymeric nanoparticle. A) Schematic of the silane attachment. B) FT-IR Spectrograph highlighting siloxane attachment to the PLNP surface. C) Schematic of the principle of Flash Nanoprecipitation for nanocomposite fabrication. D) TEM of the ZGO:Cr^{3+}@TMOS@Ps-b-PEO nanocomposite.

Flash nanoprecipitation is a nanoparticle fabrication approach that can encapsulate a range of materials into polymer nanoparticles(24). Here, we used FNP to fabricate persistent luminescent nanocomposites of ZGO:Cr^{3+}@TMOS and poly styrene-*b*-poly(ethylene) oxide (PS-*b*-PEO)(**Figure 2C&D**). Their hydrophobic core is a mixture of ZGO:Cr^{3+}@TMOS and PS while the PEO coat provides aqueous stability; though, other block copolymers can be used for fabrication (**Table S1**). Before the incorporation of sensing components, we used the ZGO:Cr^{3+}@TMOS@PS-b-PEO (shown in Figure 2C&D) to show that the autofluorescence of fetal bovine serum (FBS) can be completely omitted from our luminescence measurements (**Figure S3**). The FBS is strongly autofluorescent with a broad peak at 500 nm which overlaps with the ZGO:Cr^{3+} emission unless a time-resolved acquisition approach is used.

Optode sensor design revolves around the choice of functional components embedded in a hydrophobic polymer matrix. The ionophore, acting as the recognition unit, extracts and stabilizes the ion of choice into the nanoparticle core. At the same time, the non-fluorescent pH indicator, blueberry-C6-ester-652 (blueberry) is deprotonated and increases in absorbance, gating the PLNP emission. An ionic additive, Na^+TFPB^-, is incorporated into the sensor core to balance the positive charge on the protonated blueberry. Combining blueberry and Na^+TFPB^-, with either potassium ionophore I, sodium ionophore X, or calcium ionophore II into the FNP solvent stream yielded K^+, Na^+, or Ca^{2+} PLNs, respectively. The ion PLN emission decreases as a function of analyte concentration and blueberry absorbance (**Figure 3A-C and S4**). As expected, the addition of optode components still allowed for ZGO:Cr^{3+}@TMOS incorporation into the PLN core (**Figure S5**).

https://doi.org/10.26434/chemrxiv-2024-m0sk6 **ORCID:** https://orcid.org/0000-0002-3198-3340 Content not peer-reviewed by ChemRxiv. **License:** CC BY 4.0

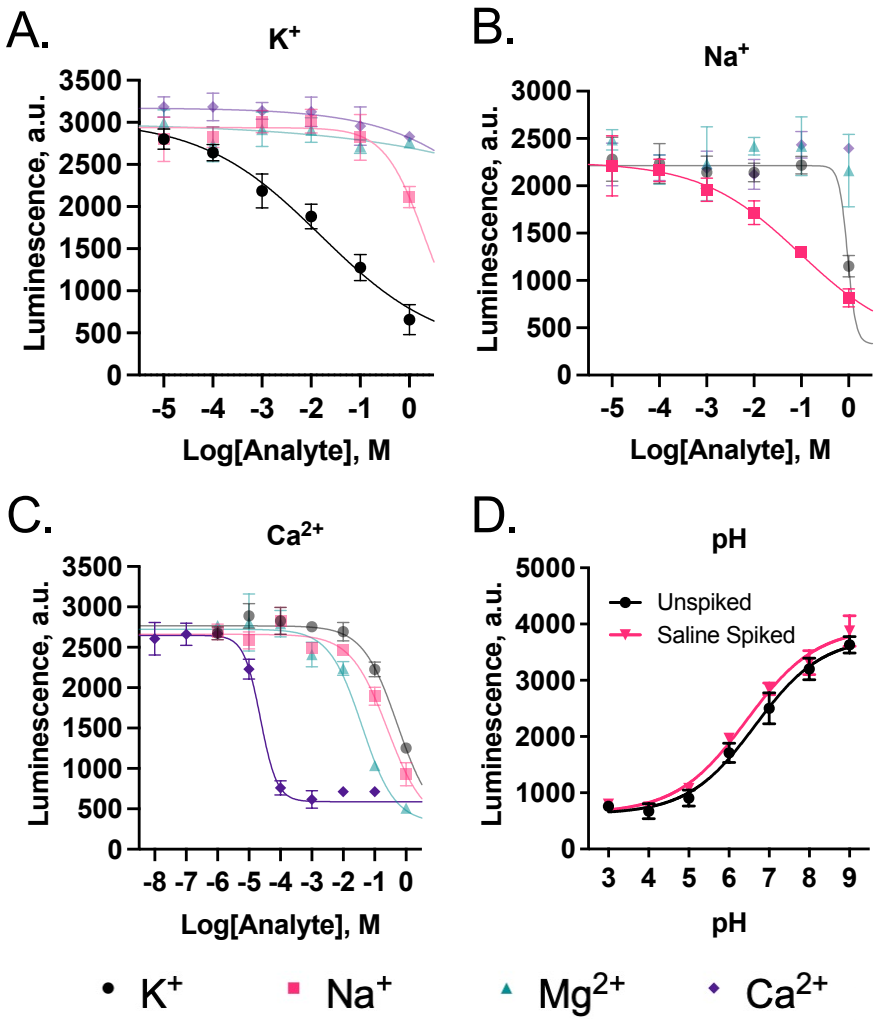

Figure 3. Calibration curves for the ion and pH persistent luminescent nanosensors. The K^+ (A), Na^+ (B), and Ca^{2+} (C) sensors were tested against common ions in separate solutions and all showed good selectivity (the target ion is darker in each panel). D) The pH PLN calibrations in Britton-Robinson Universal buffer with (pink) or without (black) saline spike (n = 3 for all calibrations).

Using a 100µs delay time, the K^+ PLNs in **Figure 3A** are 100-times more selective for K^+ than Na^+ ($\log K_{K,Na}$ = -2.1) and have a dynamic range that overlaps with concentrations found in serum(25). Importantly, the K^+ PLN response stays consistent as the delay time is increased out to 1 ms which could allow K^+ quantification in systems with fluorescent sources of variable luminescent lifetimes (e.g., when multiplexing) (**Figure S6**). The K^+ PLNs are also reversible (corroborating the expected equilibrium-based ion exchange mechanism) and have a functional lifetime of at least 8 days (**Figure S7 & S8**).

Likewise, using a 100µs delay, the Na^+ PLNs shown in **Figure 3B** have a selectivity coefficient that compares to other Na^+ sensors using the same ionophore and PEG-based surfactants ($\log K_{Na,K}$ = -1.1), which are known to impact K^+ partitioning and selectivity(26). The Na^+ PLNs have a dynamic range sufficient for serum quantification and a functional lifetime between 4 and 8 days (**Figure S9**). The Ca^{2+} PLNs (**Figure 3C,** 100µs delay) are ~1000-times more selective over the major competing ion Mg^{2+} ($\log K_{Ca,Mg}$ = -3.2) and have a functional lifetime of less than 4 days (**Figure S10**). The size and selectivity coefficients of all ion PLNs can be seen in **Tables S1** and **S2,** respectively. To further confirm the ion exchange mechanism of the ion PLNs, the ionophores were excluded from formulations, and the time-resolved response to ions was tested. As expected, without an ionophore, the sensors respond according to ion lipophilicity (Hofmeister series) (**Figure S11**). Additionally, there is no response to pH or ions when the optode components are excluded from the formulation, indicating the modulation of ZGO:Cr^{3+} emission is a function of the dye's protonation degree and selective partitioning (**Figure S12**).

https://doi.org/10.26434/chemrxiv-2024-m0sk6 **ORCID:** https://orcid.org/0000-0002-3198-3340 Content not peer-reviewed by ChemRxiv. **License:** CC BY 4.0

Adjusting the PLN formulation to incorporate a different lipophilic pH indicator, Chromoionophore II (ChII), allowed us to measure across the biological pH range with the persistent luminescence format (**Figure 3D**, 500 μs delay). The inverse relationship between pH and ChII absorbance at 700nm (**Figure S13**) results in the increasing ZGO:Cr^{3+} signal seen in **Figure 3D**. Importantly, the pH PLN response remains the same with multiple delay times (**Figure S14**) and when saline concentrations of ions are spiked into the buffered standards, indicating no significant response to ionic strength (**Figure 3D**, pink). The pH PLN signal was also tested against Na^+ and K^+ (10μM – 1M) – no change in signal occurred (**Figure S15**). Additionally, the calibrations of the pH PLNs are consistent for 8 days (**Figure S16**). Next, the pH PLN response was measured in pH-adjusted FBS from pH 3-9. An inner filter effect (IFE) impacted the sensor signal but can be adjusted for using established methods (see equation S2)(27). Using a delay-time, we can omit FBS autofluorescence and calibrate the pH PLNs in the serum while achieving the same fit parameters as the response in buffered standards (**Figure S17**). Without a delay time, these measurements are not possible in FBS as the background signal is at least 5 times that of the sensor response (**Figure S18**).

We used K^+ PLNs to quantify K^+ in FBS. After mixing the FBS with K^+ PLNs (1-to-1 v/v) and adjusting for IFE, the K^+ level was found to be 1.9 ± 0.8 mM. These results show that ion-selective PLNs are a promising tool for the evaluation of real clinical samples – even those with background autofluorescence.

To fabricate O_2-sensitive PLNs, we used the phosphorescent PdTPTBP (em: 800 nm, τ_0 = 356 μs(28)) as the O_2 indicator and the ZGO:Cr^{3+} emission as the O_2 insensitive reference (**Figure S19**) for time-resolved, ratiometric measurements. Exciting the Pd-chelate results in an electronic transition to S_1 and intersystem crossing to an excited triplet state (T_1) causing spin inversion and a forbidden transition back to S_0 – the mechanism of phosphorescence(28, 29). Molecular O_2 can collide with the dye and quench it, resulting in a lower emission intensity and luminescence lifetime(28, 29). This collisional quenching process is characterized by the Stern-Volmer relationship (**equation S3A**). Ratiometric O_2 measurements are described by a pseudo-Stern Volmer relationship (**equation S3B**) by instead plotting the quotient of the ratiometric signal (PdTPTBP/ZGO:Cr^{3+}) at 0 mg/L O_2 by the same ratio at prevailing [O_2], giving a linear response (Figure 4A, black)(30, 31). As expected, the pseudo-K_{sv} increases over the measured O_2 range by increasing the delay time – a function of the variable luminescence lifetime of PdTPTBP (Figure 4A and S20).

https://doi.org/10.26434/chemrxiv-2024-m0sk6 **ORCID:** https://orcid.org/0000-0002-3198-3340 Content not peer-reviewed by ChemRxiv. **License:** CC BY 4.0

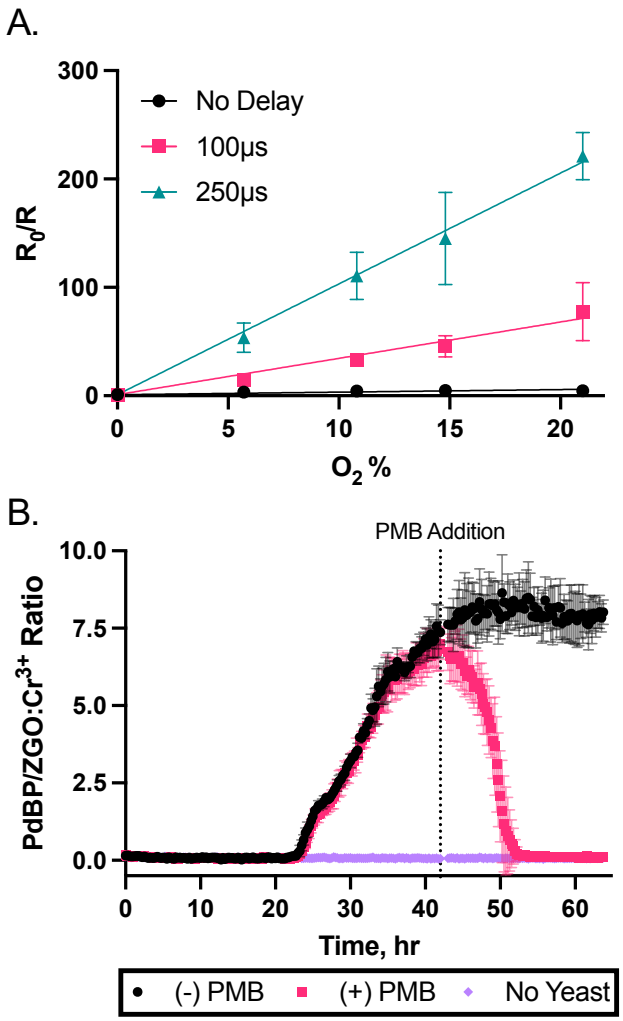

Figure 4. A) Ratiometric calibration curves of the O_2 PLNs with various delay times fit to Eq. S3B (K_{psv} = 0.236, 3.35, and 10.2 for no delay, 100µs, and 250µs, respectively. B) The O_2 PLNs can track O_2 metabolism of yeast over a 60-hour incubation with a 500 µs time gate. Metabolism is halted after adding an antimicrobial at 42 hr and the culture returns to atmospheric conditions.

While spectral separation approaches have been used to overcome autofluorescence in microbial systems (31–33), this work achieves this with ratiometric sensors that are compatible with a time-resolved measurement approach. O_2 consumption of *Saccharomyces cerevisiae* (Kolsch I) was monitored over 65 hours with the O_2 PLNs (plate setup in **Figure S21**). Without a delay, yeast autofluorescence interferes with ZGO:Cr^{3+} emission and precludes ratiometric O_2 measurements (**Figure S22A**) but using a 500 µs delay eliminates the autofluorescence and shows an increasing ratiometric signal at 20hrs (**Figure 4B and S22B**). **Figure 4B** shows that metabolic activity is inhibited upon the addition of an antimicrobial agent (potassium metabisulfite) and the O_2 concentration is brought back to baseline after 10 hrs.

In summary, our approach of integrating hydrophobic persistent luminescence nanoparticles into an optode-based nanosensor allowed for autofluorescence-free measurements in biological samples. An advantage of the ion-selective optode approach is the ability to tune dynamic range and selectivity depending on the sensing components in the polymeric matrix(15, 34). Utilizing this modularity enabled us to fabricate persistent luminescence nanosensors for five different biologically relevant analytes. While long-lifetime emissions have been used for the quantification of O_2 using phosphorescent lifetime imaging or other custom microscopes/CCD camera setups(35, 36), the systems are often expensive or difficult to build for the end user. We showed that the ratiometric O_2 PLNs can be used in a standard plate reader for facile time-resolved monitoring of O_2 consumption in a high throughput manner. Overall, we anticipate that the PLNP nanocomposite can be used as a multifunctional

https://doi.org/10.26434/chemrxiv-2024-m0sk6 **ORCID:** https://orcid.org/0000-0002-3198-3340 Content not peer-reviewed by ChemRxiv. **License:** CC BY 4.0

and highly versatile platform for autofluorescence-free sensing and imaging in a breadth of complex biological systems.

AUTHOR INFORMATION

Corresponding Author

Kevin J. Cash. kcash@mines.edu

Present Addresses

Chemical and Biological Engineering. Alderson Hall, Colorado School of Mines, Golden, CO 80401

Funding Sources

This material is based upon work supported by the National Science Foundation under Grant No. 1944204.

ACKNOWLEDGMENT

We would like to thank Sara Russo, Adam Job, and Saeed Ahmadi Vaselabadi for their help with HR-TEM and XRD. This material is based upon work supported by the National Science Foundation under Grant No. 1944204.

REFERENCES

1. Rong G, Tuttle EE, Neal Reilly A, Clark HA. 2019. Recent Developments in Nanosensors for Imaging Applications in Biological Systems. Annu Rev Anal Chem 12:109–128.

2. Doussineau T, Schulz A, Lapresta-Fernandez A, Moro A, Körsten S, Trupp S, Mohr GJ. 2010. On the Design of Fluorescent Ratiometric Nanosensors. Chem – A Eur J 16:10290–10299.

3. Saccomano SC, Jewell MP, Cash KJ. 2021. A review of chemosensors and biosensors for monitoring biofilm dynamics. Sensors and Actuators Reports 3:100043.

4. Wu S, Li Y, Ding W, Xu L, Ma Y, Zhang L. 2020. Recent Advances of Persistent Luminescence Nanoparticles in Bioapplications. Nano-Micro Lett 12:70.

5. Sun X, Song L, Liu N, Shi J, Zhang Y. 2021. Chromium-Doped Zinc Gallate Near-Infrared Persistent Luminescence Nanoparticles in Autofluorescence-Free Biosensing and Bioimaging: A Review. ACS Appl Nano Mater 4:6497–6514.

6. Shi L, Shao J, Jing X, Zheng W, Liu H, Zhao Y. 2020. Autoluminescence-Free Dual Tumor Marker Biosensing by Persistent Luminescence Nanostructures. ACS Sustain Chem Eng 8:686–694.

7. Liu J-L, Zhao X, Chen L-J, Pan L-M, Yan X-P. 2021. Dual-Emissive Persistent Luminescence Nanoparticle-Based Charge-Reversible Intelligent Nanoprobe for Persistent Luminescence-Ratio Bioimaging along with Chemo-Photothermal Synergic Therapy. Anal Chem 93:7348–7354.

8. Pan L-M, Zhao X, Wei X, Chen L-J, Wang C, Yan X-P. 2022. Ratiometric Luminescence Aptasensor Based on Dual-Emissive Persistent Luminescent Nanoparticles for Autofluorescence- and Exogenous Interference-Free Determination of Trace Aflatoxin B1 in Food Samples. Anal Chem 94:6387–6393.

9. Feng F, Chen X, Li G, Liang S, Hong Z, Wang H-F. 2018. Afterglow Resonance Energy Transfer Inhibition for Fibroblast Activation Protein-α Assay. ACS Sensors 3:1846–1854.

10. Wang J, Ma Q, Zheng W, Liu H, Yin C, Wang F, Chen X, Yuan Q, Tan W. 2017. One-Dimensional Luminous Nanorods Featuring Tunable Persistent Luminescence for Autofluorescence-Free Biosensing. ACS Nano 11:8185–8191.

11. Luo Q, Wang W, Tan J, Yuan Q. 2021. Surface Modified Persistent Luminescence Probes for Biosensing and Bioimaging: A Review. Chinese J Chem 39:1009–1021.

12. Paterson AS, Raja B, Garvey G, Kolhatkar A, Hagström AE V, Kourentzi K, Lee TR, Willson RC. 2014. Persistent Luminescence Strontium Aluminate Nanoparticles as Reporters in Lateral Flow Assays. Anal Chem 86:9481–9488.

13. Yin Z, Zhu L, Lv Z, Li M, Tang D. 2021. Persistent luminescence nanorods-based autofluorescence-free biosensor for

https://doi.org/10.26434/chemrxiv-2024-m0sk6 **ORCID:** https://orcid.org/0000-0002-3198-3340 Content not peer-reviewed by ChemRxiv. **License:** CC BY 4.0

prostate-specific antigen detection. Talanta 233:122563.

14. Mistlberger G, Crespo GA, Bakker E. 2014. Ionophore-Based Optical Sensors. Annu Rev Anal Chem 7:483–512.

15. Du X, Xie X. 2021. Ion-Selective optodes: Alternative approaches for simplified fabrication and signaling. Sensors Actuators B Chem 335:129368.

16. Sodia TZ, David AA, Chesney AP, Perri JN, Gutierrez GE, Nepple CM, Isbell SM, Cash KJ. 2021. Nanoparticle-Based Liquid–Liquid Extraction for the Determination of Metal Ions. ACS Sensors 6:4408–4416.

17. Ruckh TT, Skipwith CG, Chang W, Senko AW, Bulovic V, Anikeeva PO, Clark HA. 2016. Ion-Switchable Quantum Dot Förster Resonance Energy Transfer Rates in Ratiometric Potassium Sensors. ACS Nano 10:4020–4030.

18. Xie L, Qin Y, Chen H-Y. 2012. Polymeric Optodes Based on Upconverting Nanorods for Fluorescent Measurements of pH and Metal Ions in Blood Samples. Anal Chem 84:1969–1974.

19. Ferris MS, Chesney AP, Ryan BJ, Ramesh U, Panthani MG, Cash KJ. 2020. Silicon Nanocrystals as Signal Transducers in Ionophore-Based Fluorescent Nanosensors. Sensors Actuators B Chem 129350.

20. Galyean AA, Behr MR, Cash KJ. 2018. Ionophore-based optical nanosensors incorporating hydrophobic carbon dots and a pH-sensitive quencher dye for sodium detection. Analyst 143:458–465.

21. Wang R, Du X, Wu Y, Zhai J, Xie X. 2018. Graphene Quantum Dots Integrated in Ionophore-Based Fluorescent Nanosensors for Na+ and K+. ACS Sensors 3:2408–2414.

22. Ferris MS, Behr MR, Cash KJ. 2019. An ionophore-based persistent luminescent 'Glow Sensor' for sodium detection. RSC Adv 9:32821–32825.

23. Lin Q, Li Z, Yuan Q. 2019. Recent advances in autofluorescence-free biosensing and bioimaging based on persistent luminescence nanoparticles. Chinese Chem Lett 30:1547–1556.

24. Saad WS, Prud'homme RK. 2016. Principles of nanoparticle formation by flash nanoprecipitation. Nano Today 11:212–227.

25. Zacchia M, Abategiovanni ML, Stratigis S, Capasso G. 2016. Potassium: From Physiology to Clinical Implications. Kidney Dis 2:72–79.

26. Robinson KJ, Soda Y, Bakker E. 2022. Recent improvements to the selectivity of extraction-based optical ion sensors. Chem Commun 58:4279–4287.

27. 2006. Fluorescence Sensing BT - Principles of Fluorescence Spectroscopy, p. 623–673. *In* Lakowicz, JR (ed.), . Springer US, Boston, MA.

28. Quaranta M, Borisov SM, Klimant I. 2012. Indicators for optical oxygen sensors. Bioanal Rev 4:115–157.

29. Sodia TZ, Cash KJ. 2023. Editors' Choice—Luminescent Oxygen Sensors: Valuable Tools for Spatiotemporal Exploration of Metabolism in In Vitro Systems. ECS Sensors Plus 2:032401.

30. Jewell MP, Galyean AA, Kirk Harris J, Zemanick ET, Cash KJ. 2019. Luminescent Nanosensors for Ratiometric Monitoring of Three-Dimensional Oxygen Gradients in Laboratory and Clinical Pseudomonas aeruginosa Biofilms. Appl Environ Microbiol 85:e01116-19.

31. Saccomano SC, Cash KJ. 2022. A near-infrared optical nanosensor for measuring aerobic respiration in microbial systems. Analyst https://doi.org/10.1039/D1AN01855H.

32. Mendonsa AA, Soeldner CC, Mudd NE, Saccomano SC, Cash KJ. 2023. Triplet–Triplet Annihilation Upconversion-Based Oxygen Sensors to Overcome the Limitation of Autofluorescence. ACS Sensors 8:3043–3050.

33. Jewell MP, Greer MD, Dailey AL, Cash KJ. 2020. Triplet-Triplet Annihilation Upconversion Based Nanosensors for Fluorescence Detection of Potassium. ACS Sensors 5:474–480.

34. Ferris MS, Katageri AG, Gohring GM, Cash KJ. 2018. A dual-indicator strategy for controlling the response of ionophore-based optical nanosensors. Sensors Actuators B Chem 256:674–681.

35. Koren K, Moßhammer M, Scholz V V, Borisov SM, Holst G, Kühl M. 2019. Luminescence Lifetime Imaging of

https://doi.org/10.26434/chemrxiv-2024-m0sk6 **ORCID:** https://orcid.org/0000-0002-3198-3340 Content not peer-reviewed by ChemRxiv. **License:** CC BY 4.0

Chemical Sensors—A Comparison between Time-Domain and Frequency-Domain Based Camera Systems. Anal Chem 91:3233–3238.

36. Moßhammer M, Scholz V V, Holst G, Kühl M, Koren K. 2019. Luminescence Lifetime Imaging of O2 with a Frequency-Domain-Based Camera System. JoVE e60191.

https://doi.org/10.26434/chemrxiv-2024-m0sk6 **ORCID:** https://orcid.org/0000-0002-3198-3340 Content not peer-reviewed by ChemRxiv. **License:** CC BY 4.0

https://doi.org/10.26434/chemrxiv-2024-m0sk6 **ORCID:** https://orcid.org/0000-0002-3198-3340 Content not peer-reviewed by ChemRxiv. **License:** CC BY 4.0